remote sensing

MDPI

Article

Spatiotemporal Evolution and Driving Mechanisms of kNDVI in Different Sections of the Yangtze River Basin Using Multiple Statistical Methods and the PLSPM Model

Zhenjiang Wu [1], Fengmei Yao [1,*], Adeel Ahmad [1], Fan Deng [2,3] and Jun Fang [3,4]

[1] College of Earth and Planetary Sciences, University of Chinese Academy of Sciences, Beijing 100049, China; wuzhenjiang22@mails.ucas.ac.cn (Z.W.); adeelaadi9082@gmail.com (A.A.)
[2] School of Geoscience, Yangtze University, Wuhan 430100, China; dengfan@yangtzeu.edu.cn
[3] Hunan Provincial Key Laboratory of Geo-Information Engineering in Surveying, Mapping and Remote Sensing, Hunan University of Science and Technology, Xiangtan 411201, China; fangjun008@hnust.edu.cn
[4] National-Local Joint Engineering Laboratory of Geo-Spatial Information Technology, Hunan University of Science and Technology, Xiangtan 411201, China
* Correspondence: yaofm@ucas.ac.cn; Tel.: +86-13691221581

Abstract: Spatiotemporal vegetation changes serve as a key indicator of regional ecological environmental quality and provide crucial guidance for developing strategies for regional ecological protection and sustainable development. Currently, vegetation change studies in the Yangtze River Basin primarily rely on the Normalized Difference Vegetation Index (NDVI). However, the NDVI is susceptible to atmospheric and soil conditions and exhibits saturation phenomena in areas with high vegetation coverage. In contrast, the kernel NDVI (kNDVI) demonstrates significant advantages in suppressing background noise and improving saturation thresholds through nonlinear kernel transformation, thereby enhancing sensitivity to vegetation changes. To elucidate the spatiotemporal characteristics and driving mechanisms of vegetation changes in the Yangtze River Basin, this study constructed a temporal kNDVI using MOD09GA data from 2000 to 2022. Considering sectional heterogeneity, rather than analyzing the entire region as a whole as in previous studies, this research examined spatiotemporal evolution characteristics by sections using four statistical metrics. Subsequently, Partial Least Squares Path Modeling (PLSPM) was innovatively introduced to quantitatively analyze the influence mechanisms of topographic, climatic, pedological, and socioeconomic factors. Compared to traditional correlation analysis and the geographical detector method, PLSPM, as a theoretically driven statistical method, can simultaneously process path relationships among multiple latent variables, effectively revealing the intensity and pathways of driving factors' influences, while providing more credible and interpretable explanations for kNDVI variation mechanisms. Results indicate that the overall kNDVI in the Yangtze River Basin exhibited an upward trend, with the midstream demonstrating the most significant improvement with minimal interannual fluctuations, the upstream displaying an east-increasing and west-stable spatial pattern, and the downstream demonstrating coexisting improvement and degradation characteristics, with these trends expected to persist. Driving mechanism analysis reveals that the upstream was predominantly influenced by the climatic factor, the midstream was dominated by terrain, and the downstream displayed terrain–soil coupling effects. Based on these findings, it is recommended that the upstream focus on enhancing vegetation adaptation management to climate change, the midstream need to coordinate the relationship between topography and human activities, and the downstream should concentrate on controlling the negative impacts of urban expansion on vegetation.

check for updates

Academic Editor: Izaya Numata

Received: 11 December 2024
Revised: 5 January 2025
Accepted: 11 January 2025
Published: 16 January 2025

Citation: Wu, Z.; Yao, F.; Ahmad, A.; Deng, F.; Fang, J. Spatiotemporal Evolution and Driving Mechanisms of kNDVI in Different Sections of the Yangtze River Basin Using Multiple Statistical Methods and the PLSPM Model. *Remote Sens.* **2025**, *17*, 299. https://doi.org/10.3390/rs17020299

Copyright: © 2025 by the authors. Licensee MDPI, Basel, Switzerland. This article is an open access article distributed under the terms and conditions of the Creative Commons Attribution (CC BY) license (https://creativecommons.org/licenses/by/4.0/).

Keywords: Yangtze River Basin; kNDVI; spatiotemporal evolution; PLSPM; driving mechanisms

1. Introduction

Vegetation is a crucial component of terrestrial ecosystems, and its spatiotemporal dynamics directly reflect the quality of regional ecological environments and the evolution of land cover [1,2]. As a key element of the Earth's surface system, vegetation plays an irreplaceable role in maintaining ecological balance, regulating climate, conserving soil and water, and preserving biodiversity [3,4]. Globally, vegetation changes in several major river basins have triggered serious ecological issues. For instance, the continuous decline in forest cover in the Amazon Basin has led to sharp biodiversity loss and reduced carbon sink capacity [5], vegetation degradation in the North American Mississippi River Basin has exacerbated soil erosion [6], and variations in vegetation coverage in China's Yellow River Basin directly affect soil erosion and dust storm frequency [7]. Therefore, accurate monitoring and assessment of vegetation dynamics are crucial for understanding regional ecological environmental changes and formulating environmental protection policies [7,8], while vegetation indices serve as essential tools for quantitatively characterizing vegetation growth conditions, providing reliable technical means for vegetation monitoring [9].

The Yangtze River Basin, as one of China's most significant water systems, spans the eastern, central, and western geographical regions of China, representing a crucial area for both economic-social development and ecological environmental protection [4,10]. The vegetation growth conditions in this region directly influence ecological functions such as soil and water conservation, climate regulation, and biodiversity maintenance, forming an essential foundation for agricultural production, urban development, and ecological security along the river [11,12]. In recent years, global climate change has led to alterations in regional precipitation patterns and temperature increases, directly affecting the hydrothermal conditions for vegetation growth. Simultaneously, human activities such as urbanization, agricultural expansion, and industrial emissions have exerted pressure on the ecosystem. Under these dual effects, vegetation growth conditions in the Yangtze River Basin have undergone significant changes [4,13]. Furthermore, from upstream to downstream, the regional topography transitions from the Qinghai-Tibet Plateau and Yunnan-Guizhou Plateau to hilly basins and plains, while the climate shifts from plateau climate to subtropical monsoon climate [14]. Additionally, human activities in different sections demonstrate distinct characteristics. These variations result in significant regional differences in the spatial distribution and changing trends of vegetation within the basin, leading to diverse response mechanisms of vegetation to climate change and human activities in different sections [15,16]. Therefore, conducting section-specific vegetation change studies is of great significance for accurately understanding the vegetation dynamics and their driving mechanisms in the Yangtze River Basin. However, existing studies typically analyze the basin as a whole, overlooking the substantial differences in topography, climate, and human activities among different sections. This simplified approach limits our in-depth understanding of the distinct vegetation change characteristics and their driving mechanisms in each section, making it difficult to provide targeted scientific evidence for regional ecological protection. By adopting a sectional analysis approach, we can systematically reveal the differentiated response mechanisms of vegetation to natural and anthropogenic factors across sections, thus providing support for developing more precise ecological protection strategies. Nevertheless, such studies remain relatively scarce.

The development of remote sensing technology has provided effective means for large-scale, long-term ecosystem monitoring [14,16,17]. Using spectral information obtained through satellite remote sensing, researchers have developed various vegetation indices for vegetation monitoring [18,19]. Among these, the Normalized Difference Vegetation Index (NDVI) has become one of the most widely applied vegetation monitoring indicators due to its sensitivity to vegetation changes, easy accessibility, and strong comparability, playing a crucial role in global vegetation dynamics monitoring, phenological change research, and ecosystem assessment [20–22]. However, the NDVI's effectiveness is limited by its susceptibility to atmospheric and soil background interference, as well as signal saturation in high vegetation coverage areas [23]. To overcome these limitations, researchers developed the Enhanced Vegetation Index (EVI) and Near-Infrared Reflectance of Vegetation (NIRv). While these improved indices enhanced sensitivity to vegetation structure and photosynthetic activity, they have not fully resolved the signal saturation issue in high coverage areas [24]. In response, the recently developed kernel Normalized Difference Vegetation Index (kNDVI), based on kernel method theory, employs nonlinear kernel functions to capture higher-order relationships between spectral bands. Compared to other indices, the kNDVI maintains better response capability in high vegetation coverage areas, demonstrates superior performance in monitoring key vegetation parameters such as the Leaf Area Index (LAI), and exhibits enhanced stability and noise resistance across spatial and temporal scales [25,26]. Studies have shown that kNDVI possesses stronger vegetation monitoring capabilities than traditional indices like the NDVI [23,27]. However, research utilizing this index to study vegetation changes in the Yangtze River Basin remains limited. Conducting such research would contribute to a deeper understanding of vegetation change characteristics and their driving mechanisms in this region.

Vegetation change results from the combined effects of multiple factors, including climatic conditions, topographic features, soil properties, and human economic activities. These driving factors not only directly influence vegetation changes but also exhibit complex interactions and feedback mechanisms among themselves [28,29]. Therefore, accurately identifying and quantifying the mechanisms of various driving factors requires appropriate analytical methods. Current commonly used analysis methods face challenges in interpreting such complex driving mechanisms: traditional correlation analysis, while operationally simple, can only reveal statistical associations between variables and struggles to construct systematic causal relationship networks [30]; the geographical detector, although capable of quantitatively evaluating the explanatory power of individual factors, has limitations in handling complex theoretical frameworks with latent variables [31].

Partial Least Squares Path Modeling (PLSPM), as a theory-driven statistical method, has distinct advantages in analyzing the driving mechanisms of vegetation change. First, PLSPM can construct and validate complex pathway relationships involving multiple latent variables, quantifying both the intensity and pathways of various driving factors' effects on vegetation change [32,33]. Second, PLSPM effectively addresses multicollinearity among variables by extracting orthogonal principal components to construct latent variables and incorporating path analysis methods, thus enhancing model stability [34,35]. Furthermore, PLSPM constructs model structures based on rigorous theoretical hypotheses, enabling the analytical results to better reflect the actual mechanisms of vegetation change rather than mere statistical correlations [36]. These characteristics establish PLSPM as a powerful tool for investigating complex driving mechanisms of vegetation change, providing scientifically sound and practically meaningful evidence for ecosystem management and decision-making.

Based on the above context, this study selected the Yangtze River Basin as the study area and constructed a time-series kNDVI dataset spanning from 2000 to 2022. The kNDVI

variations were investigated using Theil–Sen slope estimation, the Mann–Kendall test, the coefficient of variation, and the Hurst index, while the PLSPM model was employed to analyze the driving mechanisms of kNDVI changes in different sections. The objectives of this study were to (1) analyze the spatiotemporal characteristics of kNDVI changes in the upstream, midstream, and downstream of the Yangtze River Basin, (2) reveal the influence mechanisms and interactions of climatic, edaphic, topographic, and socioeconomic factors on kNDVI variations across different sections, and (3) propose targeted recommendations for ecological environmental protection based on the research findings. The results of this study can provide a scientific basis for evaluating the effectiveness of ecological engineering projects in the Yangtze River Basin and formulating regionally differentiated strategies for ecological environmental protection.

2. Materials and Methods

2.1. Study Area

The Yangtze River Basin (24.5°–35.75°N, 90.55°–122.42°E) encompasses an area of approximately 1.8 million km^2 and extends over 6300 km, representing one of China's most significant river systems [37]. The basin exhibits a three-step topographical distribution, with elevation gradually decreasing from west to east. The upstream section, characterized by the Qinghai-Tibet Plateau, is dominated by plateaus and mountainous terrain, featuring rapid river flows and rich biodiversity. The midstream section primarily consists of plains with well-developed river networks, serving as a crucial agricultural production base for China. The downstream section is typified by the Yangtze River Delta, characterized by low-lying terrain and home to major metropolitan areas such as Nanjing, Hangzhou, and Shanghai, which have emerged as population centers and economic hubs [38]. From a climatological perspective, the Yangtze River Basin spans multiple climate zones, transitioning from plateau-mountain climate in the upstream section to subtropical monsoon climate in the midstream and downstream sections. The basin's average annual precipitation is approximately 1000 mm, with a notably uneven seasonal distribution where summer rainfall accounts for over 60% of the annual total. Spatially, precipitation exhibits a distinct geographical gradient, decreasing from approximately 2400 mm in the eastern downstream regions to about 300 mm in the upstream headwater areas. This significant temporal and spatial variation in precipitation significantly contributes to the basin's frequent droughts and floods [39]. Figure 1 presents the sectional map [40], land cover map [41], and elevation map of the Yangtze River Basin.

2.2. Data Acquisition and Processing

In this study, a total of 19 observational variables were employed, with data sources detailed in Table 1. Specifically, the MOD09GA and TerraClimate datasets were utilized using their annual means from 2000 to 2022. For China's 1 km grid GDP and population distribution dataset, which were only available for the years 2000, 2005, 2010, 2015, and 2020, this study applied each five-year node value to represent its corresponding five-year period (e.g., GDP data from 2000 was applied to 2000–2004, and so forth) to enable year-by-year analysis from 2000 to 2022. Although SRTMGL1_003 topographic data was only available for 2007, considering the typically minimal variation in topographic features, this dataset was applied across the entire study period. Similarly, soil classification and organic carbon data were available as single-period datasets. These were derived from machine learning predictions based on accumulated soil profile data (approximately 150,000 samples) and multi-year averaged remote sensing and climate covariates, representing a long-term stable soil distribution pattern [42]. Therefore, this dataset was also applied across the entire study period. After feature extraction, to maximize the preservation of spatial details in

the dependent variable kNDVI, which is crucial for accurately assessing vegetation change characteristics, all features were resampled to match the kNDVI's spatial resolution of 500 m for subsequent analyses.

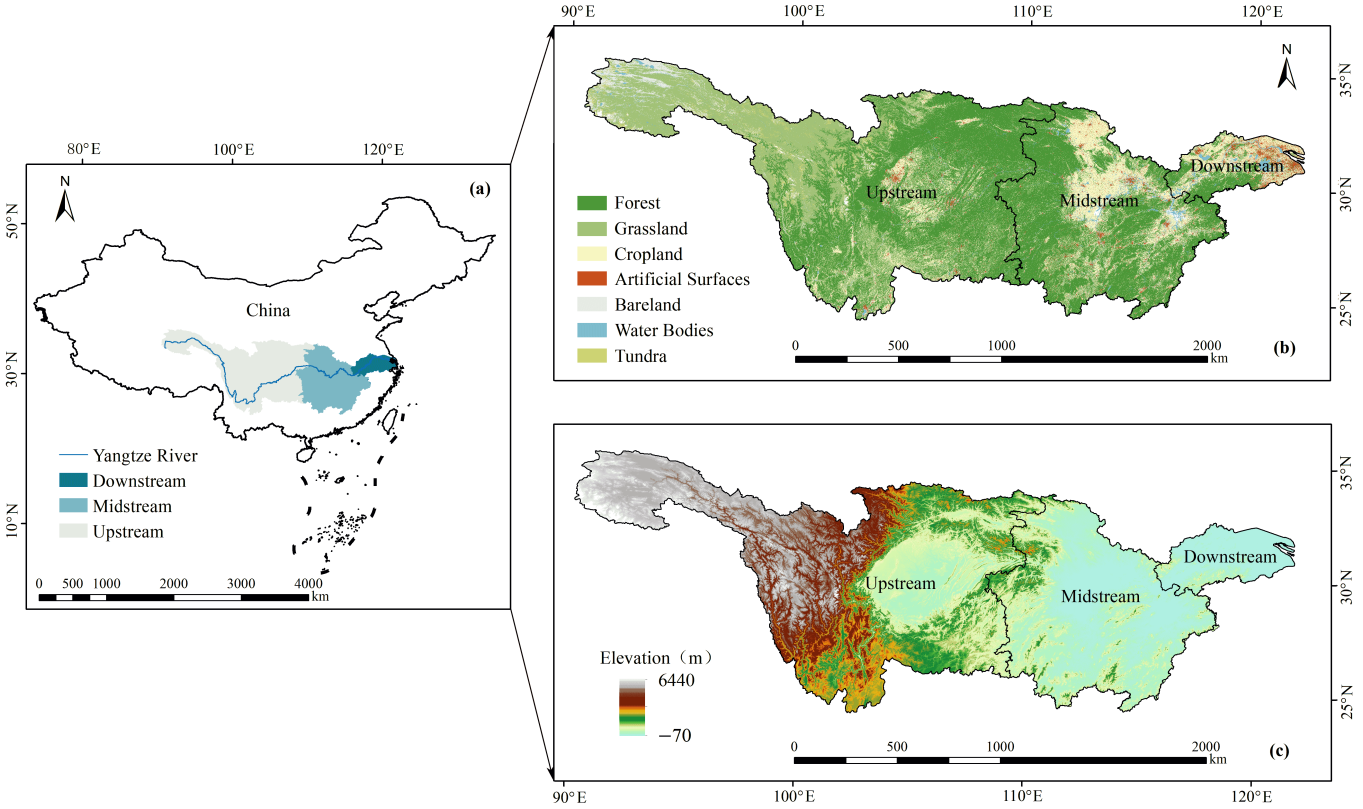


Figure 1. Sectional map (**a**), land cover map (**b**), and elevation map (**c**) of the Yangtze River Basin.

Table 1. Data sources and applications.

Datasets	Spatial Resolution	Sources	Applications and Abbreviations
MOD09GA	500 m	United States Geological Survey (https://www.usgs.gov/, accessed on 8 September 2024)	kNDVI Calculation
TerraClimate	4 km	University of California Merced (https://www.climatologylab.org/terraclimate.html, accessed on 5 July 2024)	Climate Variables Obtained: runoff (ro), ActualEvapotranspiration (aet), Reference Evapotranspiration (pet), Precipitation Accumulation (pr), Climate Water Deficit (def), Minimum Temperature (tmmn), Downward Surface Shortwave Radiation (srad), Maximum Temperature (tmmx), Soil Moisture (soil), Vapor Pressure (vap), Vapor Pressure Deficit (vpd), Wind Speed at 10 m (vs)
China's 1 km Grid GDP and Population Distribution Dataset	1 km	Resource and Environmental Science Data Platform (https://www.resdc.cn/Default.aspx, accessed on 9 September 2024)	Socioeconomic Variables Obtained: Gross Domestic Product (gdp) and Population Density (pop)
SRTMGL1_003	30 m	United States Geological Survey (https://www.usgs.gov/, accessed on 8 September 2024)	Terrain Variables Obtained: Elevation (DEM), Slope (slpoe), and Aspect (aspect)
OpenLandMap Soil OrganicCarbon Content, USDA Soil Taxonomy Great Groups	250 m	EnvirometriX (https://envirometrix.nl/, accessed on 15 September 2024)	Soil Variables Obtained: Soil Organic Carbon Content (soc) and Soil Class (soilclass)

2.3. Methods

2.3.1. Construction of Time-Series kNDVI Data (2000–2022)

This study utilized the red and near-infrared bands from the MOD09GA dataset spanning 2000–2022 to calculate the annual kNDVI values. The kNDVI, as an improved vegetation index, enhances sensitivity to vegetation changes through the introduction of nonlinear kernel functions.The calculation was performed using the following equation [23]:

$$\text{kNDVI} = tanh\left(\left(\frac{n-r}{2\sigma}\right)^2\right) \tag{1}$$

where *tanh* represents the hyperbolic tangent function, and n and r denote the reflectance values of near-infrared and red bands, respectively. Based on mathematical and eco-physiological analyses, Camps-Valls et al. proposed setting σ as the mean value of near-infrared and red wavelength bands [23], specifically $\sigma = 0.5(n + r)$. This modification leads to a simplified version of the kNDVI calculation method, expressed as $\text{kNDVI} = tanh(\text{NDVI}^2)$. As evident from the aforementioned equation, for identical spectral reflectance values, kNDVI values are demonstrably lower than NDVI values. Consequently, after considering the existing classification criteria for the NDVI in previous research [31], we established five categorical levels for kNDVI values: low values (kNDVI < 0.1), medium-low values ($0.1 \leq$ kNDVI < 0.2), medium values ($0.2 \leq$ kNDVI < 0.3), medium-high values ($0.3 \leq$ kNDVI < 0.4), and high values (kNDVI $\geq$ 0.4).

2.3.2. Theil–Sen Slope Estimation and Mann–Kendall (MK) Test

The Theil–Sen slope estimation method is commonly employed to calculate trends in time-series data. This method computes the slope between all possible pairs of time points and uses their median as the final estimate, making it robust against outliers [43]. For the time-series kNDVI data, the Theil–Sen slope estimator β is calculated as

$$\beta = \text{Median}\left(\frac{kNDVI_j - kNDVI_i}{j-i}\right) \tag{2}$$

where $kNDVI_j$ and $kNDVI_i$ represent the kNDVI values at time points j and i, respectively. A positive β indicates an increasing trend, while a negative value suggests a decreasing trend.

The MK test complements the Theil–Sen estimation by assessing the statistical significance of the kNDVI temporal trends [44]. The test statistic S is computed as

$$S = \sum_{i=1}^{n-1} \sum_{j=i+1}^{n} \text{sign}(kNDVI_j - kNDVI_i) \tag{3}$$

where the function *sign* is used to compare the kNDVI values between two time points:

$$sign(kNDVI_j - kNDVI_i) = \begin{cases} 1, & kNDVI_j > kNDVI_i \\ 0, & kNDVI_j = kNDVI_i \\ -1, & kNDVI_j < kNDVI_i \end{cases} \tag{4}$$

To evaluate the significance of S, the standardized statistic Z is calculated as follows:

$$Z = \begin{cases} \frac{S-1}{\sqrt{VAR(S)}}, & S > 0 \\ 0, & S = 0 \\ \frac{S+1}{\sqrt{VAR(S)}}, & S < 0 \end{cases} \tag{5}$$

where $VAR(S)$ represents the variance of S, typically calculated as

$$VAR(S) = \frac{n(n-1)(2n+5)}{18} \tag{6}$$

where n denotes the sample size.

When $|Z|$ exceeds a certain critical value, it indicates a significant trend in the temporal kNDVI series. In this study, the critical values were set at ±1.96 (a significance level of 0.05). Based on these parameters, evaluation criteria were established to assess the temporal trends in the kNDVI (Table 2), where the threshold of β was set to the standard deviation of Sen's slope rather than 0 to avoid misidentifying data fluctuations caused by measurement errors and data noise as significant trends.

Table 2. Classification of temporal kNDVI change trends.

β	Z	kNDVI Change Trend Classification
$\geq$Threshold	$Z \geq 1.96$	Significant Increase
$\geq$Threshold	$-1.96 < Z < 1.96$	Slight Increase
$-$Threshold $< \beta <$ threshold	Any Value	Stable
$\leq -$Threshold	$-1.96 < Z < 1.96$	Slight Decrease
$\leq -$Threshold	$Z \leq -1.96$	Significant Decrease

2.3.3. Coefficient of Variation (CV)

CV is a dimensionless metric greater than 0 that evaluates the relative dispersion of data. It is calculated by dividing the standard deviation of temporal data by its mean. A higher CV value indicates more pronounced fluctuations in temporal kNDVI data, while a lower value suggests greater stability [45]. Based on the classification criteria of the coefficient of variation from previous studies and considering that the kNDVI exhibits stronger responses to vegetation changes compared to traditional vegetation indices [4,23], this study categorized the stability of kNDVI time series into five levels: highly stable (CV < 0.1), stable ($0.1 \leq$ CV < 0.15), minor fluctuation ($0.15 \leq$ CV < 0.2), moderate fluctuation ($0.2 \leq$ CV < 0.25), and unstable (CV $\geq$ 0.25).

2.3.4. Hurst Index

The Hurst index is a measure used to evaluate the persistence of trends in temporal data [46]. It is typically calculated through Rescaled Range Analysis (R/S) [47], expressed as

$$\text{Hurst} = \frac{log(R/S)}{log(n)} \tag{7}$$

where R/S can be represented as

$$\frac{R}{S} = \frac{max_{1\leq p\leq n}(\sum_{i=1}^{p}(kNDVI_i - \frac{1}{n}\sum_{i=1}^{n} kNDVI_i)) - min_{1\leq p\leq n}(\sum_{i=1}^{p}(kNDVI_i - \frac{1}{n}\sum_{i=1}^{n} kNDVI_i))}{\sqrt{\frac{1}{n}\sum_{i=1}^{n}(kNDVI_i - \frac{1}{n}\sum_{i=1}^{n} kNDVI_i)^2}} \tag{8}$$

where $kNDVI_i$ represents the i-th value of the temporal kNDVI data, while n denotes the length of the time series. The operators $max()$ and $min()$, respectively, compute the maximum and minimum values of the expression within the parentheses as p iterates from 1 to n, where p serves as the iterator.

Hurst index ranges from 0 to 1. When Hurst = 0.5, it indicates no correlation between future and past trends in the temporal data. When Hurst < 0.5, it suggests anti-persistence, implying that future trends will be opposite to past trends. When Hurst > 0.5, it indicates long-term persistence, suggesting that future trends will continue to follow past

patterns [46]. In this study, we established a classification system by coupling the Theil–Sen slope estimator with the Hurst index to evaluate the persistence of kNDVI trends (Table 3).

Table 3. Classification of future temporal kNDVI change trends.

β	Hurst	Future kNDVI Change Trend Classification
≥threshold	>0.5	Persistent Increase
≥threshold	<0.5	Change from Increase to Decrease
−threshold < β < threshold	>0.5	Stable
Any value	=0.5	Uncertain
−threshold < β < threshold	<0.5	Uncertain
≤−threshold	>0.5	Persistent Decrease
≤−threshold	<0.5	Change from Decrease to Increase

2.3.5. The PLSPM Model

PLSPM is a structural equation modeling estimation method commonly employed for analyzing and interpreting complex causal relationships among variables. PLSPM consists of two components: the structural model and the measurement model. The structural model delineates path relationships between latent variables, revealing how these variables interact with and influence each other, thereby establishing the internal causal mechanisms within the system [48]. The measurement model defines the relationships between latent variables and their observed indicators, ensuring that latent variables accurately reflect the characteristics represented by multiple observed indicators [49]. Through the synergistic operation of these two components, PLSPM effectively analyzes complex multivariate relationships, providing in-depth understanding and quantitative analysis of latent structures [50].

The measurement model can be expressed as

$$\eta = \sum_{i=1}^{n} \lambda_i X_i + \varepsilon \tag{9}$$

where η represents the latent variable, X_i and λ_i denote the i-th manifest variable and its corresponding weight respectively, ε represents the error term, and n is the number of manifest variables.

The structural model can be expressed as

$$\text{kNDVI} = \sum_{j=1}^{m} \beta_j \eta_j + \zeta \tag{10}$$

where kNDVI is the response variable in this study, η_i and β_i represent the j-th latent variable and its path coefficient respectively, ζ denotes the error term, and m is the number of latent variables.

To ensure that the PLSPM model effectively explains the causal relationships among variables, this study employed bootstrap resampling with 1000 iterations to obtain robust statistical results. The reliability and validity of the measurement model were examined after modeling. The Dillon–Goldstein's rho (rho) is utilized to assess reliability, where higher values indicate better internal consistency among observed variables within latent variables, typically requiring a threshold above 0.6. The average variance extracted (AVE) is employed to evaluate convergent validity, with values exceeding 0.5 indicating that latent variables are well represented by their measurement variables. The structural model should be validated through the significance testing of path coefficients, where p-values less than 0.05 indicate statistical significance of the paths [50]. Additionally, the variance inflation factor (VIF) of latent variables needed to be examined, with values less than 5 indicating the absence of significant multicollinearity among latent variables [51].

Through the examination of these multiple indicators, including reliability, validity, path coefficient significance, and VIF values, the appropriateness of model construction could be determined.

After validating model validity, PLSPM generates path coefficients and various effect values [49]. Path coefficients reflect the strength and direction of direct relationships between variables. Based on these coefficients, direct, indirect, and total effects can be further calculated. Specifically, direct effects are equivalent to path coefficients between variables, while indirect effects are computed through multiple path coefficients via mediating variables. Total effects represent the sum of direct and indirect effects. The absolute magnitude of effect values indicates the strength of influence, with positive values suggesting promotional effects and negative values indicating inhibitory effects. Through these quantitative results, the relative importance of different driving factors and their influence mechanisms can be systematically revealed.

3. Results

3.1. Analysis of kNDVI Temporal Trends in the Yangtze River Basin from 2000 to 2022

Figure 2 illustrates the annual mean kNDVI variation trends across the entire Yangtze River Basin and its three sections from 2000 to 2022. The analysis reveals that the kNDVI throughout the entire basin exhibited a linear increasing trend (slope = 0.00221) over this 23-year period, with an R^2 value of 0.78 indicating high trend stability. Among the three sections, the midstream demonstrated the most rapid increase (slope = 0.00267) with stable trending characteristics (R^2 = 0.76). The upstream (slope = 0.00206, R^2 = 0.71) and downstream (slope = 0.00196, R^2 = 0.64) also displayed positive trends, although greater fluctuation was observed in the latter.

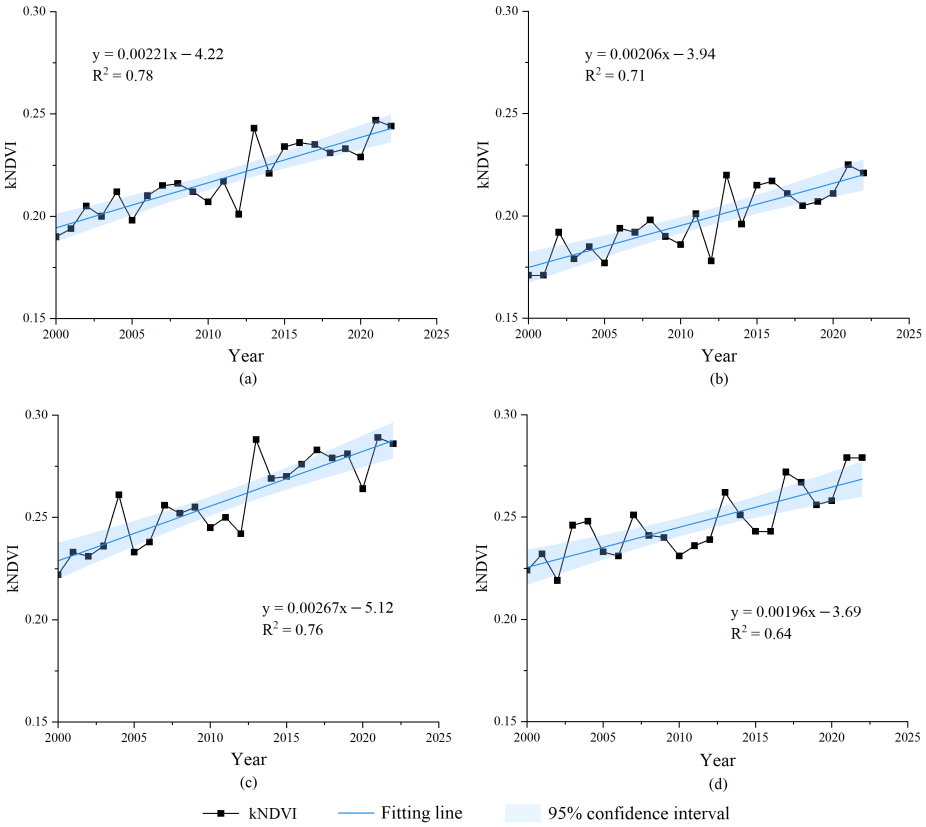


Figure 2. Line charts of kNDVI changes from 2000 to 2022 in the entire Yangtze River Basin (**a**), upstream (**b**), midstream (**c**), and downstream (**d**).

From a spatial distribution perspective (Figure 3a,b), the kNDVI values in 2000 displayed a distinct east-high and west-low pattern across the Yangtze River Basin. By 2022, while maintaining this general spatial distribution pattern, most areas showed significant improvement in kNDVI values, particularly in the eastern upstream and midstream regions. In contrast, the Qinghai-Tibet Plateau region in the western upstream maintained relatively low values. Regarding the proportional changes in kNDVI categories (Figure 3c), the high-value areas exhibited a fluctuating upward trend over the 23-year period, increasing from nearly 0% in 2000 to approximately 5% in 2022. The medium-high value areas showed steady growth, with particularly notable increases after 2012. The medium-low value areas demonstrated a continuous declining trend, decreasing from approximately 40% in 2000 to about 15% in 2022. The proportions of medium and low values remained relatively stable.

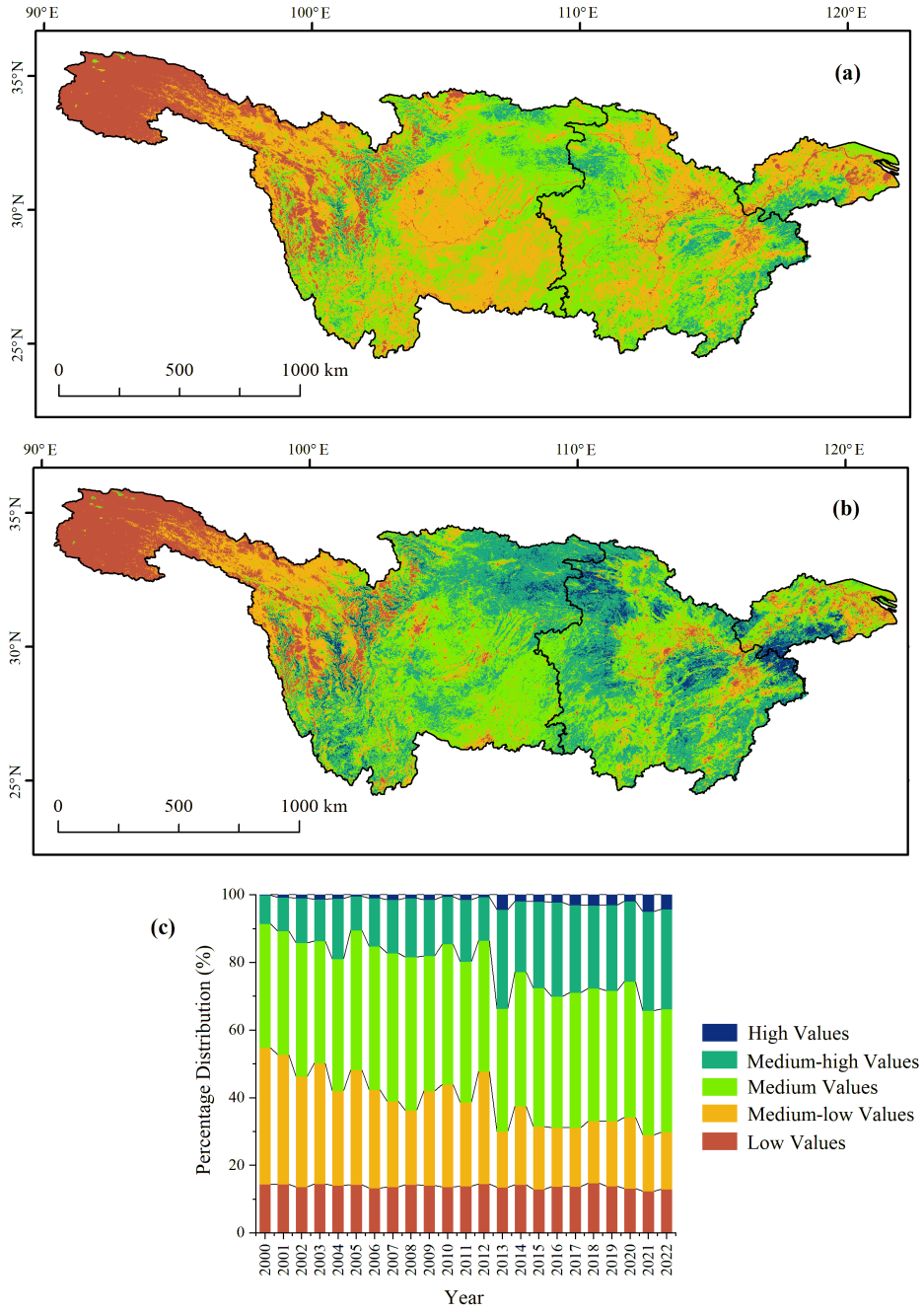


Figure 3. Spatial distribution of the kNDVI in the Yangtze River Basin in (**a**) 2000 and (**b**) 2022, and (**c**) the percentage distribution of different kNDVI categories from 2000 to 2022.

Figure 4 presents the trend analysis results obtained through Theil–Sen slope estimation and the Mann–Kendall test of the temporal kNDVI. The results indicate that, while the kNDVI showed an overall increasing trend across the basin during this period, the midstream exhibited the most significant improvement. The midstream had the highest proportions of both significant and slight increases among the three sections, with total improvement covering 83.7% of the area and only 3.7% showing decline. In the upstream, 61.1% of the area showed an increasing trend, primarily concentrated in the eastern region, while the western region remained largely stable. Although 62.1% of the downstream experienced increased kNDVI, it also had the highest proportion of degradation (14.8%) among the three sections.

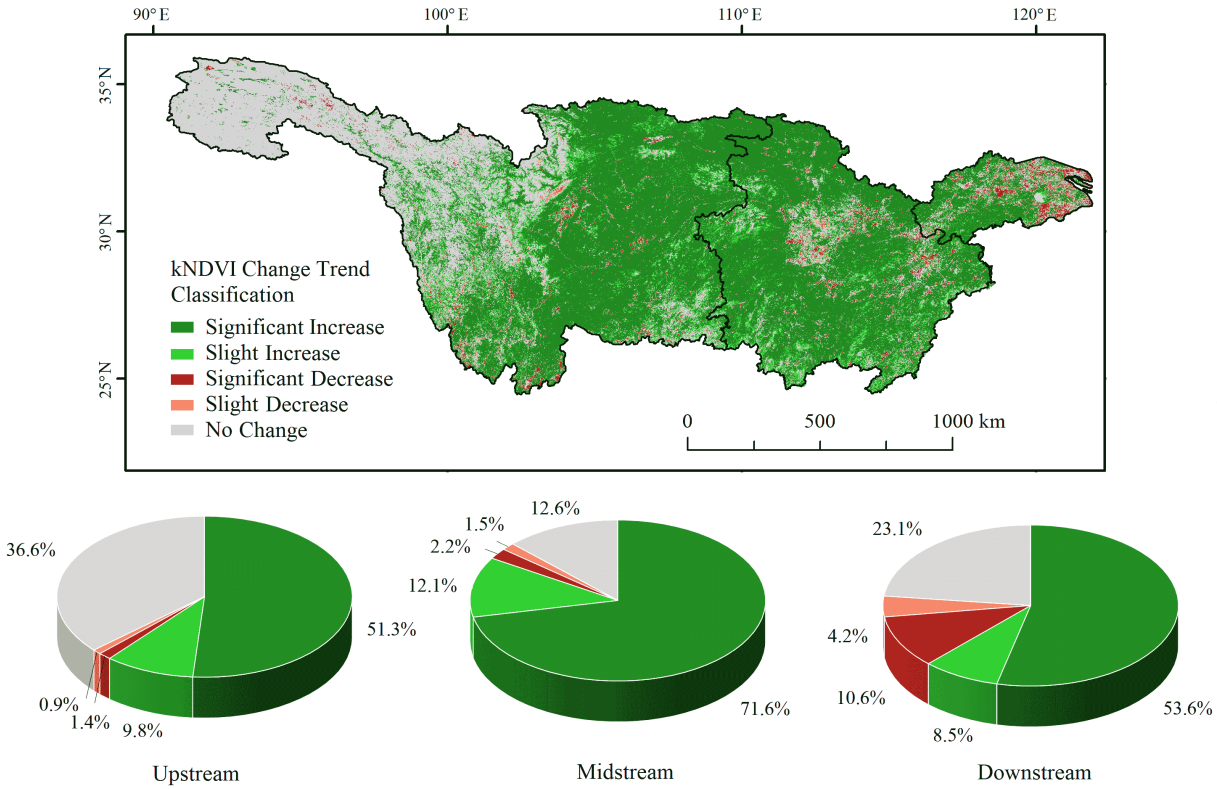


Figure 4. Temporal trends of kNDVI in the Yangtze River Basin from 2000 to 2022.

3.2. Analysis of kNDVI Variation Stability in the Yangtze River Basin from 2000 to 2022

Spatially (Figure 5), the kNDVI variations from 2000 to 2022 demonstrated generally high stability across the Yangtze River Basin, though with distinct patterns across the three sections. The midstream exhibited the highest stability, with stable and highly stable areas accounting for 76.6% of the total area. The upstream showed a cumulative stability of 61.7% (18.7% highly stable and 43% stable areas), while also containing the highest proportion of slight fluctuation areas (26.4%), indicating lower stability compared to the midstream. The downstream displayed marked spatial heterogeneity in kNDVI variation stability, featuring both the highest proportion of highly stable areas (29.1%) and the highest proportion of unstable areas (13.7%). Overall, the midstream showed the most stable kNDVI variations, while the downstream exhibited the most pronounced instability, and the upstream demonstrated moderate levels of fluctuation.

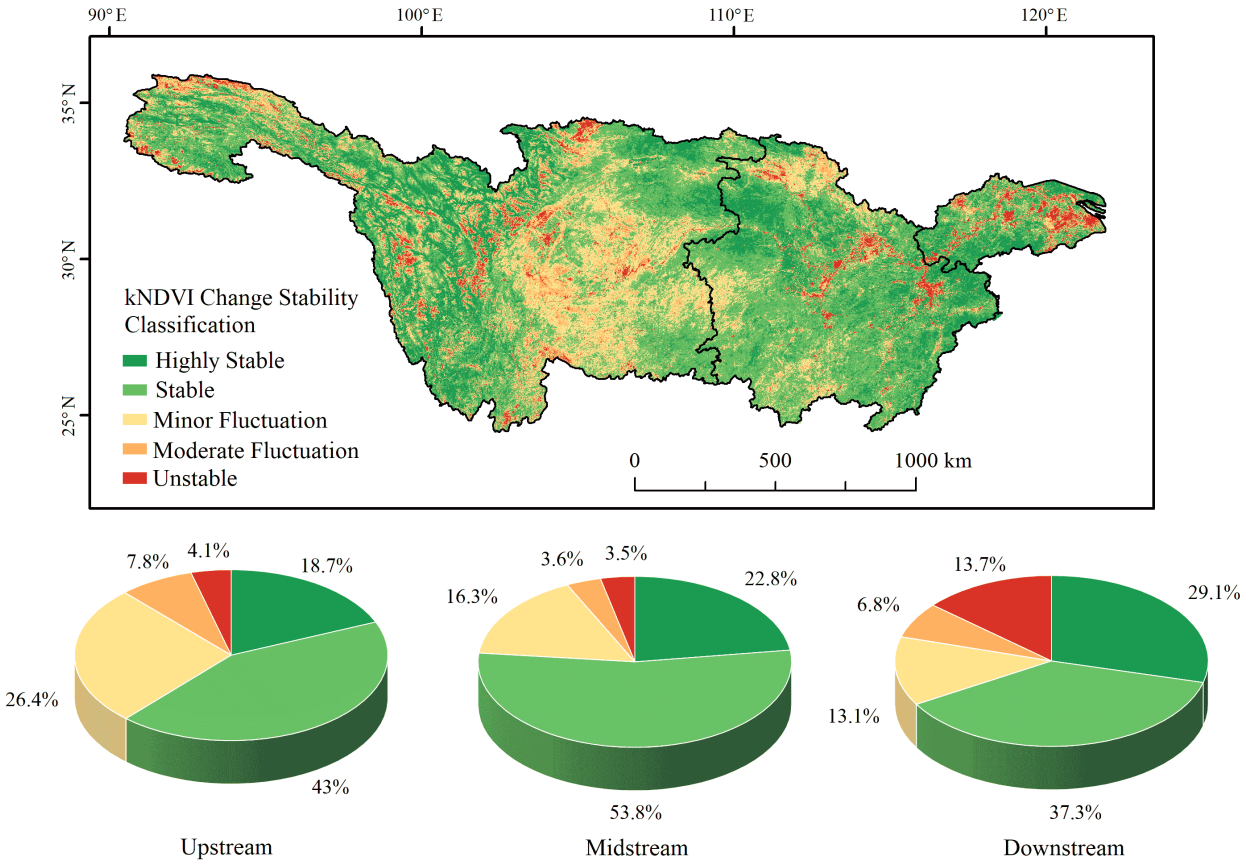


Figure 5. Stability of kNDVI variations in the Yangtze River Basin from 2000 to 2022.

3.3. Analysis of kNDVI Future Trends in the Yangtze River Basin

The analysis of future kNDVI trends in the Yangtze River Basin (Figure 6) indicates that, while the overall kNDVI is expected to maintain an upward trajectory, distinct regional variations are observed among the upstream, midstream, and downstream sections. In the midstream, areas projected to experience continuous growth in the kNDVI account for a substantial 81.5% of the section, exhibiting spatially continuous distribution, while areas expected to maintain stability constitute 9.7%, with zones of uncertain changes and other fluctuations representing minimal proportions. The upstream demonstrates more complex characteristics of change; although areas of continuous growth remain predominant (58.2%), regions maintaining stability occupy a considerable proportion (24.8%), and this section exhibits the highest percentage of areas with uncertain changes among the three sections. The downstream is primarily characterized by continuous growth, accounting for 60.4%, accompanied by 19.9% of areas maintaining stability—proportions comparable to those of the upstream. However, it is noteworthy that this section contains a significant 14.7% of areas showing continuous decline, substantially higher than both the upstream and midstream sections, with these declining areas primarily concentrated in the eastern coastal regions. In conclusion, while future kNDVI trends in the Yangtze River Basin are predominantly characterized by continuous growth, significant spatial heterogeneity exists across sections, with the midstream exhibiting the most pronounced trend of continuous growth, whereas the upstream shows higher uncertainty proportions, and the downstream demonstrates greater proportions of continuous decline.

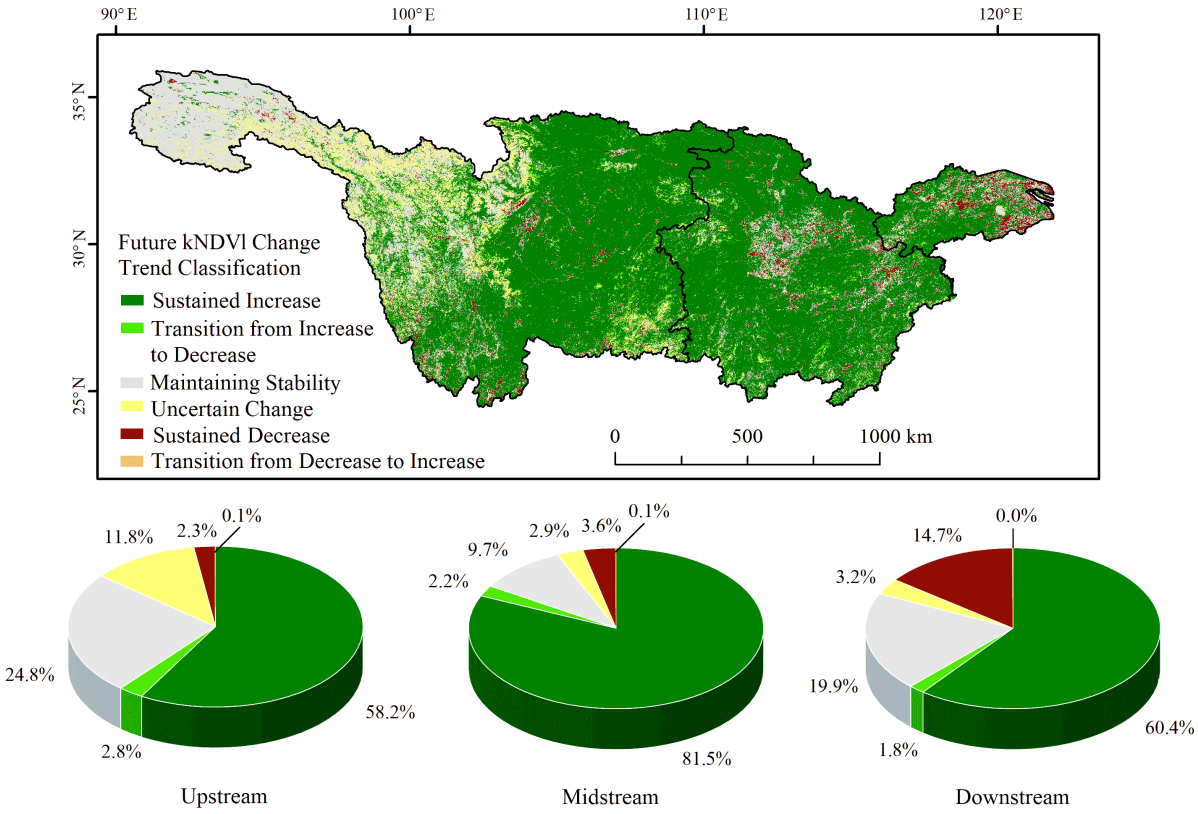


Figure 6. Future trends in the kNDVI for the Yangtze River Basin.

3.4. Analysis of kNDVI Change Driving Mechanisms Based on the PLSPM Model

This study categorized the variables in Table 1 into four latent variables: terrain, climate, social economy, and soil, with the observed variables for each latent variable presented in Table 4. Based on existing research achievements [52–54], the structural model framework of the latent variables was designed as shown in Figure 7.

Table 4. Observed variables within each latent variable.

Latent Variables	Observed Variables
Terrain	dem, slope, aspect
Climate	aet, def, pet, pr, srad, tmmn, tmmx, vap, vpd, vs
Social Economy	gdp, pop
Soil	ro, soil, soc, soilclass

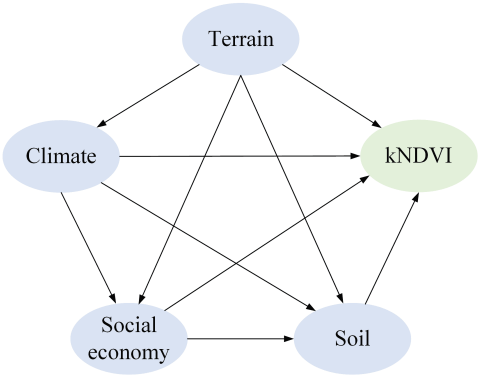


Figure 7. Framework of the structural model.

After fitting the variables in Table 4 using PLSPM, we conducted a comprehensive evaluation of the model fit. For the measurement model, all rho coefficients exceeded 0.6, with most values above 0.8 (Table A1), indicating strong internal consistency among observed variables within each latent variable. The AVE values of all latent variables surpassed the critical threshold of 0.5, confirming that the observed variables effectively explained the characteristics of the latent variables. Regarding the structural model, significance tests for all path coefficients yielded p-values less than 0.05, with the majority being less than 0.001 (Table A2), demonstrating statistically significant relationships between latent variables. Additionally, all VIF values for the latent variables were below 5 (Table A3), suggesting the absence of severe multicollinearity among variables. These results collectively validated that our PLSPM models constructed for upstream, midstream, and downstream sections all demonstrated satisfactory overall model fit.

The quantitative analysis of direct and indirect effects of terrain, climatic, socioeconomic, and soil factors on kNDVI across the three sections (Figure 8 and Table 5) revealed distinct sectional patterns. In the upstream section, the climate factor exhibited the strongest influence on kNDVI with a total effect of 0.7164, comprising a dominant direct effect of 0.6815 and an indirect effect of 0.0349 through soil and other factors. The topographic and soil factors also demonstrated positive influences on kNDVI, albeit with relatively weaker intensities, showing total effects of only 0.2285 and 0.1295, respectively. The socioeconomic factor, however, displayed a negative impact, comprising a direct effect of −0.1265 and an indirect effect of 0.0055, resulting in a total negative effect of −0.121.

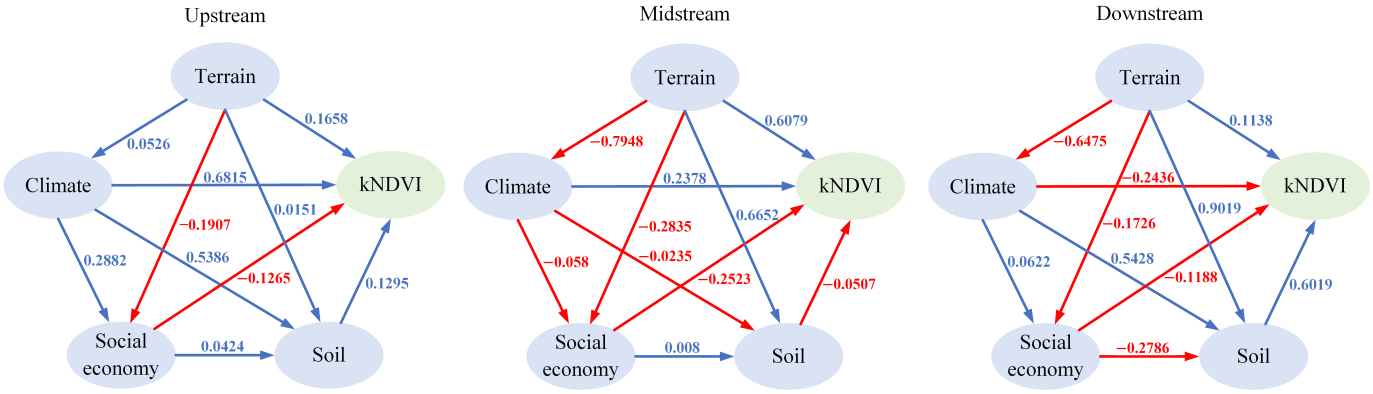


Figure 8. Path coefficients diagram of the structural model in the upstream, midstream, and downstream of the Yangtze River.

Table 5. Direct, Indirect, and Total Effects of Latent Variables on kNDVI in Upstream, Midstream, and Downstream Sections.

Path	Upstream			Midstream			Downstream		
	Direct	**Indirect**	**Total**	**Direct**	**Indirect**	**Total**	**Direct**	**Indirect**	**Total**
Terrain → Climate	0.0526	0	0.0526	−0.7948	0	−0.7948	−0.6475	0	−0.6475
Terrain → Social Economy	−0.1907	0.0157	−0.175	−0.2835	0.0461	−0.2374	−0.1726	−0.0402	−0.2128
Terrain → Soil	0.0151	0.0209	0.036	0.6652	0.0168	0.682	0.9019	−0.2922	0.6097
Terrain → kNDVI	0.1658	0.0627	0.2285	0.6079	−0.1637	0.4442	0.1138	0.55	0.6638
Climate → Social Economy	0.2882	0	0.2882	−0.058	0	−0.058	0.0622	0	0.0622
Climate → Soil	0.5386	0.0122	0.5508	−0.0235	−0.0004	−0.0239	0.5428	−0.0173	0.5255
Climate → kNDVI	0.6815	0.0349	0.7164	0.2378	0.0158	0.2536	−0.2436	0.3089	0.0653
Social Economy → Soil	0.0424	0	0.0424	0.008	0	0.008	−0.2786	0	−0.2786
Social Economy → kNDVI	−0.1265	0.0055	−0.121	−0.2523	−0.0004	−0.2527	−0.1188	−0.1677	−0.2865
Soil → kNDVI	0.1295	0	0.1295	−0.0507	0	−0.0507	0.6019	0	0.6019

In the midstream section, the influence patterns of various factors on kNDVI underwent significant changes. Unlike the upstream section, terrain became dominant, with a significant direct effect (0.6079). Although this effect was attenuated by the combined action of multiple indirect pathways (−0.1637), its total effect remained substantial at 0.4442. The climate factor exhibited relatively weak direct effects on kNDVI (0.2378), and the supplementation through indirect pathways was limited, resulting in a total effect of only 0.2537. The effect of soil on kNDVI in the midstream differed from that in the upstream, showing a negative value but with minimal impact (−0.0507). The socioeconomic factor continued to demonstrate negative influences on the kNDVI, with their total effect (−0.2527) primarily consisting of direct effects and showing notably higher intensity compared to the upstream.

In the downstream section, the mechanisms of various factors exhibit new characteristics. The topographic factor primarily influences the kNDVI through indirect pathways. Despite its relatively weak direct effect (0.1138), its total effect increases to 0.6638 through significantly impacting the soil factor (0.9019) and subsequent soil-mediated effects on the kNDVI, highlighting soil's crucial mediating role in terrain–kNDVI interactions. The soil factor demonstrates the second strongest total effect of 0.6019, following terrain. Although the climate factor shows negative direct effects on the kNDVI (−0.2436), it exerts positive regulatory influences through alternative pathways, particularly via soil-mediated positive effects on the kNDVI, ultimately resulting in a weak positive total effect (0.0652). The socioeconomic factor affects the kNDVI through both direct (−0.1188) and indirect (−0.1677) pathways, with its total effect (−0.2865) being significantly higher than those observed in the upstream and midstream.

4. Discussion

4.1. Spatiotemporal Characteristics of kNDVI Changes in the Yangtze River Basin

The results of this study demonstrate that the kNDVI in the Yangtze River Basin exhibited an overall increasing trend from 2000 to 2022, indicating the effectiveness of ecological restoration and vegetation management initiatives in the region. This improvement trend parallels the vegetation enhancement observed in the Yellow River Basin during the same period; however, the former exhibited notably higher improvement rates, which may be attributed to the Yangtze River Basin's abundant precipitation and more favorable climatic conditions [55]. Nevertheless, this vegetation improvement displays distinct spatial heterogeneity across the Yangtze River Basin, with the midstream section showing the most pronounced enhancement, where 83.7% of the area demonstrated growth trends and exhibited the highest stability, with stable and highly stable regions accounting for 76.6%. This remarkable improvement can be attributed to the large-scale implementation of the Grain for Green Program and the advancement of ecological corridor construction in the midstream urban agglomeration [56].

The kNDVI in the upstream section exhibits a distinct spatial pattern characterized by increases in the east and stability in the west. The growth observed in the eastern areas may be attributed to the implementation of major ecological barrier construction projects in the upper Yangtze River [13]. In contrast, the western plateau region shows limited vegetation growth and maintains a relatively stable state, which is primarily due to harsh natural conditions (mean annual temperature below 0 °C, thin air, intense ultraviolet radiation, and scarce precipitation) that restrict vegetation growth [57,58]. Additionally, the ecosystem in this region is predominantly composed of alpine meadows and steppes, with vegetation dominated by dwarf cold-resistant species and relatively simple community structures, which further constrain significant vegetation growth [59,60]. Notably, this section demonstrates a high proportion of areas with minor fluctuations (26.4%), which

can be primarily attributed to the region's unique terrain–climate–vegetation coupling mechanism. The dramatic topographical changes from the Qinghai-Tibet Plateau to the Sichuan Basin have led to modifications in large-scale weather system transport pathways through blocking and lifting effects [61,62]. Furthermore, variations in terrain characteristics, including elevation, slope, and aspect, have induced changes in surface energy balance and local circulation patterns, resulting in significant spatial heterogeneity in multiple climatic parameters, including temperature, precipitation, radiation, humidity, and wind speed [63]. These climatic parameters do not influence vegetation growth independently but rather form a climate system through complex interactions [64]. Within this system, the interconnected effects and feedback mechanisms among climatic elements mean that even minor variations in individual climate variables can be amplified through internal system feedback, potentially exerting more substantial impacts on vegetation. This terrain–climate–vegetation coupling mechanism renders vegetation more sensitive to environmental changes.

The downstream section demonstrated the most complex change characteristics. While 62.1% of the area achieved vegetation improvement, 14.8% experienced degradation, reflecting the profound contradiction between urbanization processes and ecological conservation [65]. The spatial differentiation in change stability was most pronounced in this section, encompassing both the highest proportion of highly stable areas (29.1%) and unstable areas (13.7%). This complexity primarily stems from the ongoing interplay between intensive human activities and ecological conservation requirements, particularly pronounced in the Yangtze River Delta economic zone [66,67]. In fact, this coexistence of improvement and degradation is also commonly observed in other economic zones at the river estuaries, such as the Pearl River Delta. However, compared to the latter, the former has demonstrated a significantly higher proportion of vegetation improvement areas in recent years [68], indicating that the former has achieved more substantial progress in balancing economic development and environmental protection through more effective ecological management measures.

The analysis of kNDVI future trends in the Yangtze River Basin exhibit similar patterns of spatial heterogeneity. The midstream section, currently showing the best vegetation growth status, also presents the most promising future trends, with an anticipated 81.5% of the area maintaining sustained growth trends and displaying strong spatial continuity, suggesting that the section's advantageous natural conditions and effective conservation measures will continue to exert positive influences on vegetation status improvement. The pattern of eastern growth and western stability in the upstream section is expected to persist, with continuous growth dominating (58.2%) despite a significant proportion of stable areas (24.8%). This section also shows the highest percentage of uncertain changes, which aligns with the previously discussed high sensitivity of its vegetation ecosystem to climate change. The complexity currently observed in the downstream section is projected to intensify further, and although 60.4% of the area is expected to maintain continuous growth, a notably high proportion (14.7%) of areas, primarily concentrated in the eastern coastal regions, shows persistent decline. These findings suggest that the conflict between urbanization processes and ecological conservation will continue to pose challenges, necessitating particular attention in regional development planning.

4.2. Multi-Factor Driving Mechanisms of kNDVI Changes in the Yangtze River Basin

The quantitative analysis of PLSPM modeling reveals distinct driving mechanisms of kNDVI variations across different sections of the Yangtze River Basin. In the upstream, vegetation changes are primarily controlled by natural factors, among which the climate

factor demonstrates the most significant impact, while the terrain factor, despite its positive influence, exerts relatively weak effects. This phenomenon is closely associated with the coupling mechanism of terrain–climate–vegetation in this region. As discussed in Section 4.1, the complex topographical variations in this region result in high spatial heterogeneity of the climate variables, which interact to form a sophisticated climate system. The synergistic effects among climate variables within this system amplify the changes of individual variables, ultimately leading to enhanced vegetation sensitivity to climate change. Additionally, the soil factor contributes positively to vegetation growth, albeit with relatively weak influence intensity, which may be attributed to the generally thin soil layers and low soil development levels in this section [69]. Notably, although human activities are relatively limited in this section overall, the socioeconomic factor still exhibits negative impacts, reflecting potential threats to vegetation growth from hydraulic engineering projects and mineral resource exploitation [70]. However, compared to the midstream and downstream, the negative impacts of human activities in the upstream section are minimal, which aligns with the characteristics of low population density and weak development intensity in this area [71].

In the midstream, the topographic factor plays a dominant role, which is associated with the extensive plains in this section (Figure 1c). The Jianghan Plain and Dongting Lake Plain, serving as the major geomorphological units in this section, feature flat terrain that reduces soil erosion and facilitates water retention and nutrient preservation, thereby creating favorable conditions for vegetation growth [72]. However, the flat topography has also facilitated economic activities such as urbanization and agricultural development, slightly attenuating the positive effects of topography on vegetation growth [73]. The impact intensity of the climatic factor on vegetation in this section is relatively weak, which correlates with the regional topographic characteristics. Unlike the dramatic climatic variations caused by complex terrain in the upstream, the midstream plains have fostered a relatively homogeneous spatial distribution pattern of climate, diminishing the differential regulatory effects of the climatic factor on vegetation [74]. The soil factor demonstrates a slight inhibitory effect on vegetation, attributed to the long-term agricultural development that has resulted in soil quality degradation, consequently imposing minor negative impacts on vegetation growth [75]. The negative impact of the socioeconomic factor on vegetation in the midstream is notably stronger than in the upstream, correlating with the terrain characteristics that facilitate development. The flat topographic conditions have established the midstream as a crucial zone for human activities. Intensive agricultural production, urban construction, and industrial development have directly altered the original vegetation patterns, imposing significant pressure on vegetation systems [76].

Vegetation changes in the downstream section exhibit characteristics predominantly driven by the coupling of the topographic and soil factors. Similar to the midstream, the flat and open topographic conditions in the downstream have facilitated vegetation growth to some extent [77]. More importantly, the gentle terrain in this section has reduced surface runoff velocity and enhanced soil water infiltration capacity. It has also facilitated the deposition of sediments from the upstream and midstream, particularly in areas such as the Yangtze River Delta alluvial plain, forming deep and fertile soils that provide excellent growth media for vegetation [78]. This significant regulatory effect of terrain on soil development, combined with the direct support of both terrain and soil for vegetation growth, constitutes the positive coupling effect of the terrain–soil factors on vegetation growth in this section. The climatic factor exhibits complex mechanisms in the downstream. Frequent heavy rainfall, typhoons, and extreme high temperatures have negative impacts on vegetation growth [79]. However, the subtropical monsoon

climate has simultaneously improved soil fertility and fungal diversity by regulating the soil environment (e.g., soil moisture, pH) and resource supply (e.g., root exudates, organic matter), indirectly promoting vegetation growth [80]. Consequently, the climatic factor demonstrates a weak positive effect on vegetation. The socioeconomic factor exerts the most significant negative impact on downstream vegetation, which is inextricably linked to the region's intensive human activities. As one of China's most economically developed regions, the lower reaches of the Yangtze River, especially the Yangtze River Delta, accommodate extensive urban construction and industrial development, resulting in significant impacts on vegetation growth [40,81]. These impacts manifest not only through direct land-use conversion driven by urban planning expansion and land market development, but also through indirect effects on vegetation growth via industrial pollutant emissions, urban stormwater runoff, and extensive surface hardening, which lead to soil nutrient loss and contamination [82]. These mechanisms explain the significant direct and indirect negative effects of the socioeconomic factor on vegetation growth.

The above findings indicate that the spatiotemporal evolution of the kNDVI in the Yangtze River Basin is driven by the combined effect of multiple factors, necessitating section-specific strategies for ecological conservation and economic development. The downstream section should adopt successful experiences from the Pearl River Delta's "Three Lines and One List" ecological zoning control system, strengthening soil and water conservation while improving soil quality alongside economic advancement. Specific measures include restricting unnecessary industrial and agricultural expansion to minimize ecosystem disturbance, thereby achieving sustainable and coordinated development of ecology and economy [83]. The midstream section should focus on optimizing soil conditions, drawing from the Yellow River's midstream experience in vegetation restoration and economic activity regulation [84]. Through scientific planning, this section should control the impact of excessive development on vegetation, promoting soil quality enhancement and healthy vegetation growth. The upstream section can learn from the vegetation protection measures implemented in the Three Rivers Source Region, such as grassland rotation and adaptive grazing [85], while referencing the comprehensive soil and water conservation practices of the Jinsha River [86]. By combining engineering measures with biological approaches, this section can mitigate the negative impacts of climate change and enhance ecosystem resilience.

4.3. Contributions and Limitations of This Study

This study makes three major contributions in terms of methodological applications and research findings. First, novel discoveries were obtained through the application of the kNDVI. Compared to previous studies using traditional vegetation indices such as the NDVI, this research yielded similar results regarding the overall vegetation improvement trend in the Yangtze River Basin and the most significant improvement in the midstream [4,87], thus validating the reliability of our findings. Moreover, the kNDVI-based analysis reveals new features. For example, in areas with high vegetation coverage, such as the midstream and downstream sections of the Yangtze River, the traditional NDVI tends to saturate, making it difficult to detect subtle vegetation changes. In contrast, this study provides a more detailed characterization of these changes, particularly highlighting a nuanced coexistence pattern of improvement and degradation in the downstream [16]. In areas where background noise significantly interferes, such as the upstream plateau regions, traditional indices are often influenced by soil background and atmospheric conditions. Instead, the kNDVI-based analysis in this study more accurately captures the spatial pattern of eastern increase and western stability, a differential trend rarely identified in previous studies. Second, this study addressed the limitations of traditional whole-scale research by

conducting driving force analysis by sections. This approach thoroughly considered the differences in natural geographical features and socioeconomic development levels among the upstream, midstream, and downstream sections, thereby more accurately reflecting the unique characteristics of vegetation changes in each section. For instance, the study found that the upstream was primarily influenced by the climatic factor, while the midstream was predominantly affected by the topographic factor, and the downstream exhibited characteristics dominated by terrain–soil coupling. These regional differences highlight the significant value of sectional analysis. Third, the introduction of the PLSPM model for driving force analysis demonstrated notable advantages over traditional correlation analysis and the geographical detector method [12,36]. As a theory-driven statistical method, PLSPM not only processes complex path relationships among multiple latent variables simultaneously but also effectively identifies direct and indirect effects, thus providing a more comprehensive revelation of the driving mechanism. For example, in the downstream, this study discovered that the terrain factor exerted significant indirect effects through the soil factor, a complex influence pathway that would be difficult to accurately identify and quantify using traditional methods [88].

Nevertheless, several limitations of this study warrant further discussion. The first concerns the method of research unit division. Although meaningful results were achieved by dividing the river into upstream, midstream, and downstream sections, alternative spatial divisions, such as those based on tributary systems (including the Jialing River system, Jinsha River system, and Han River system), might yield different conclusions. This suggests that future research could consider adopting multiple spatial division perspectives, as different spatial division approaches possess distinct characteristics and may be more effective in capturing and analyzing specific ecological processes, thereby enabling a more comprehensive understanding of the spatial heterogeneity in vegetation dynamics [89]. The second limitation relates to data constraints. Due to difficulties in obtaining certain data, such as annual GDP, data from proximate years were used to substitute for missing data. Regarding spatial resolution, considering the importance of preserving kNDVI spatial details for accurate assessment of vegetation change characteristics, all data were resampled to 500 m to maintain consistency with kNDVI data. Furthermore, although MOD09GA data has undergone atmospheric and geometric corrections [90], and we employed annual averaging to reduce errors from sensor and atmospheric condition fluctuations, and the lower spatial resolution somewhat mitigated the effects of topographical conditions, the original data quality issues, along with data substitution treatments and resampling processes, may still influence the research results. To address these data limitations, future studies could consider constructing more complete datasets, employing more advanced data fusion methods, and incorporating field observation data for validation to enhance the reliability of research findings. Finally, due to the lack of high temporal resolution continuous observation data, monthly-scale driving force analysis could not be conducted, potentially overlooking seasonal characteristics and short-term response mechanisms of vegetation changes [10]. Therefore, future research could consider developing high-performance data interpolation methods to obtain high temporal resolution data and constructing monthly-scale driving force analysis frameworks to better reveal seasonal response mechanisms of vegetation to environmental changes.

5. Conclusions

Based on the kNDVI data from 2000 to 2022 in the Yangtze River Basin, this study investigated the spatiotemporal characteristics of vegetation changes and their driving mechanisms. The main conclusions obtained were as follows:

- The vegetation in the Yangtze River Basin has shown an overall improvement trend, albeit with significant regional disparities. The midstream section has demonstrated the most substantial improvement with the highest stability. The upstream section has exhibited a spatial pattern characterized by improvement in the east and stability in the west, while the downstream section has displayed a complex pattern of coexisting improvement and degradation. In the future, these regional disparities are expected to persist.
- Analyses based on the PLSPM models have revealed differentiated driving mechanisms across sections: the upstream section is predominantly influenced by the climatic factor, reflecting its high vegetation sensitivity to climate change; the midstream section is mainly controlled by the topographic factor while being significantly affected by human activities; the downstream section is characterized by coupled terrain–soil dominance and experiences the strongest pressure from socioeconomic development.
- Based on these findings, differentiated ecological protection strategies are recommended for different sections: the upstream should prioritize enhancing vegetation resilience to climate change; the midstream needs to balance topographic conditions with human activities; the downstream should focus on controlling the negative impacts of urban expansion while strengthening soil environment protection.

These findings provide scientific evidence for understanding the dynamics and causes of vegetation changes in the Yangtze River Basin, offering valuable references for formulating section-specific ecological and environmental protection policies.

Author Contributions: Conceptualization, Z.W. and F.Y.; methodology, Z.W.; software, Z.W.; validation, F.Y., A.A. and F.D.; formal analysis, Z.W.; investigation, F.D. and J.F.; resources, F.Y. and F.D.; data curation, Z.W., F.Y. and A.A.; writing—original draft preparation, Z.W.; writing—review and editing, Z.W. and F.Y.; visualization, A.A.; supervision, F.Y.; project administration, F.Y. and F.D.; funding acquisition, F.Y., F.D. and J.F. All authors have read and agreed to the published version of the manuscript.

Funding: This work was supported by the National Key Research and Development Program of China (No. 2023YFF1303601), the General Program of National Natural Science Foundation of China (No. 42071425), and the Open Fund of Hunan Provincial Key Laboratory of Geo-Information Engineering in Surveying, Mapping and Remote Sensing, Hunan University of Science and Technology (No. E2240).

Data Availability Statement: The data are available on request.

Conflicts of Interest: The authors declare no conflicts of interest.

Appendix A

Table A1. Reliability and validity assessment of the PLSPM models.

	Evaluation Metrics	Terrain	Climate	Social Economy	Soil
Upstream	rho	0.67	0.94	0.98	0.77
	AVE	0.51	0.79	0.95	0.63
Midstream	rho	0.91	0.92	0.97	0.86
	AVE	0.83	0.7	0.95	0.74
Downstream	rho	0.94	0.89	0.98	0.88
	AVE	0.89	0.63	0.96	0.78

Table A2. Significance levels of path coefficients in the PLSPM models.

Path	Upstream	Midstream	Downstream
Terrain → Climate	**	**	**
Terrain → Social Economy	**	**	**
Terrain → Soil	**	**	**
Terrain → kNDVI	**	**	**
Climate → Social Economy	**	**	**
Climate → Soil	**	**	**
Climate → kNDVI	**	**	**
Social Economy → Soil	**	*	**
Social Economy → kNDVI	**	**	**
Soil → kNDVI	**	**	**

Note: * indicates $p < 0.05$, ** indicates $p < 0.001$.

Table A3. VIF values of latent variables.

	Terrain	Climate	Social Economy	Soil	kNDVI
Upstream	1.11	2.64	1.17	1.48	2.43
Midstream	4.14	2.8	1.15	1.87	1.39
Downstream	3.86	2.65	1.29	3.62	2.98

References

1. Caparros-Santiago, J.A.; Rodriguez-Galiano, V.; Dash, J. Land surface phenology as indicator of global terrestrial ecosystem dynamics: A systematic review. *ISPRS J. Photogramm. Remote Sens.* **2021**, *171*, 330–347. [CrossRef]
2. Frappart, F.; Wigneron, J.; Li, X.; Liu, X.; Al-Yaari, A.; Fan, L.; Wang, M.; Moisy, C.; Masson, E.; Lafkih, Z.A.; et al. Global Monitoring of the Vegetation Dynamics from the Vegetation Optical Depth (VOD): A Review. *Remote Sens.* **2020**, *12*, 2915. [CrossRef]
3. Jones, H.G.; Vaughan, R.A. *Remote Sensing of Vegetation: Principles, Techniques, and Applications*; Oxford University Press: New York, NY, USA, 2010; pp. 68–69.
4. Qu, S.; Wang, L.; Lin, A.; Yu, D.; Yuan, M.; Li, C. Distinguishing the impacts of climate change and anthropogenic factors on vegetation dynamics in the Yangtze River Basin, China. *Ecol. Indic.* **2020**, *108*, 105724. [CrossRef]
5. Phillips, O.L.; Lewis, S.L.; Baker, T.R.; Chao, K.J.; Higuchi, N. The changing Amazon forest. *Philos. Trans. R. Soc. B Biol. Sci.* **2008**, *363*, 1819–1827. [CrossRef] [PubMed]
6. Olson, K.R.; Gennadiyev, A.N.; Zhidkin, A.P.; Markelov, M.V. Impact of land use change and soil erosion in upper Mississippi River Valley on soil organic carbon retention and greenhouse gas emissions. *Soil Sci.* **2011**, *176*, 449–458. [CrossRef]
7. Wang, N.; Zhang, Q.; Sun, S.; Yang, W.; Zhang, Y.; Zhai, Y.; Liu, H.; Wang, H.; He, M.; Fan, P.; et al. Sandstorms in the Yellow River Basin, China in the 21st century: Spatiotemporal pattern and variation trend. *Ecol. Indic.* **2023**, *154*, 110601. [CrossRef]
8. Tian, F.; Liu, L.Z.; Yang, J.H.; Wu, J.J. Vegetation greening in more than 94% of the Yellow River Basin (YRB) region in China during the 21st century caused jointly by warming and anthropogenic activities. *Ecol. Indic.* **2021**, *125*, 107479. [CrossRef]
9. Xue, J.; Su, B. Significant remote sensing vegetation indices: A review of developments and applications. *J. Sens.* **2017**, *2017*, 1353691. [CrossRef]
10. Wang, Q.; Ju, Q.; Wang, Y.; Fu, X.; Zhao, W.; Du, Y.; Jiang, P.; Hao, Z. Regional Patterns of Vegetation Dynamics and Their Sensitivity to Climate Variability in the Yangtze River Basin. *Remote Sens.* **2022**, *14*, 5623. [CrossRef]
11. Chen, F.; Lin, A.; Zhu, H.; Niu, J. Quantifying Climate Change and Ecological Responses within the Yangtze River Basin, China. *Sustainability* **2018**, *10*, 3026. [CrossRef]
12. Guo, R.; Cai, A.; Chen, X. The quantitative effects of climate change and human activity on the vegetation growth in the Yangtze River Basin. *Front. Earth Sci.* **2023**, *11*, 1168384. [CrossRef]
13. Qu, S.; Wang, L.; Lin, A.; Zhu, H.; Yuan, M. What drives the vegetation restoration in Yangtze River basin, China: Climate change or anthropogenic factors? *Ecol. Indic.* **2018**, *90*, 438–450. [CrossRef]
14. Fu, J.; Liu, J.; Qin, J.; Yang, L.; Zhang, Z.; Deng, Y.; Hu, Y.; Su, B. Monitoring long-term vegetation dynamics over the Yangtze River Basin, China, using multi-temporal remote sensing data. *Ecosphere* **2024**, *15*, e4809. [CrossRef]
15. Zhang, J.; Zhang, Y.; Sun, G.; Song, C.; Li, J.; Hao, L.; Liu, N. Climate Variability Masked Greening Effects on Water Yield in the Yangtze River Basin During 2001–2018. *Water Resour. Res.* **2021**, *58*, e2021WR030382. [CrossRef]
16. Yi, L.; Sun, Y.; Ouyang, X.; Yin, S. Identifying the Impacts of Climate Change and Human Activities on Vegetation Cover Changes: A Case Study of the Yangtze River Basin, China. *Int. J. Environ. Res. Public Health* **2022**, *19*, 6239. [CrossRef]

17. Pettorelli, N.; to Bühne, H.S.; Tulloch, A.; Dubois, G.; Macinnis-Ng, C.; Queirós, A.; Keith, D.; Wegmann, M.; Schrodt, F.; Stellmes, M.; et al. Satellite remote sensing of ecosystem functions: Opportunities, challenges and way forward. *Remote Sens. Ecol. Conserv.* **2018**, *4*, 71–93. [CrossRef]
18. Toth, C.; Jóźków, G. Remote sensing platforms and sensors: A survey. *ISPRS J. Photogramm. Remote Sens.* **2016**, *115*, 22–36. [CrossRef]
19. Wang, R.; Gamon, J.A. Remote sensing of terrestrial plant biodiversity. *Remote Sens. Environ.* **2019**, *231*, 111218. [CrossRef]
20. Li, S.; Xu, L.; Jing, Y.; Yin, H.; Li, X.; Guan, X. High-quality vegetation index product generation: A review of NDVI time series reconstruction techniques. *Int. J. Appl. Earth Obs. Geoinf.* **2021**, *105*, 102640. [CrossRef]
21. Ozyavuz, M.; Bilgili, B.; Salici, A. Determination of vegetation changes with NDVI method. *J. Environ. Prot. Ecol.* **2015**, *16*, 264–273.
22. Beck, H.E.; McVicar, T.R.; van Dijk, A.I.; Schellekens, J.; de Jeu, R.A.; Bruijnzeel, L.A. Global evaluation of four AVHRR–NDVI data sets: Intercomparison and assessment against Landsat imagery. *Remote Sens. Environ.* **2011**, *115*, 2547–2563. [CrossRef]
23. Camps-Valls, G.; Campos-Taberner, M.; Moreno-Martínez, Á.; Walther, S.; Duveiller, G.; Cescatti, A.; Mahecha, M.D.; Muñoz-Marí, J.; García-Haro, F.J.; Guanter, L.; et al. A unified vegetation index for quantifying the terrestrial biosphere. *Sci. Adv.* **2021**, *7*, eabc7447. [CrossRef] [PubMed]
24. Merrick, T.; Pau, S.; Detto, M.; Broadbent, E.; Bohlman, S.A.; Still, C.; Zambrano, A.A.A. Unveiling spatial and temporal heterogeneity of a tropical forest canopy using high-resolution NIRv, FCVI, and NIRvrad from UAS observations. *Biogeosciences* **2021**, *18*, 6077–6091. [CrossRef]
25. Wang, Q.; Moreno-Martínez, Á.; Muñoz-Marí, J.; Campos-Taberner, M.; Camps-Valls, G. Estimation of vegetation traits with kernel NDVI. *ISPRS J. Photogramm. Remote Sens.* **2023**, *195*, 408–417. [CrossRef]
26. Chen, Z.; Zhang, X.; Jiao, Y.; Cheng, Y.; Zhu, Z.; Wang, S.; Zhang, H. Investigating the spatio-temporal pattern evolution characteristics of vegetation change in Shendong coal mining area based on kNDVI and intensity analysis. *Front. Ecol. Evol.* **2023**, *11*, 1344664. [CrossRef]
27. Guo, B.; Zhang, R.; Lu, M.; Xu, M.; Liu, P.; Wang, L. A New Large-Scale Monitoring Index of Desertification Based on Kernel Normalized Difference Vegetation Index and Feature Space Model. *Remote Sens.* **2024**, *16*, 1771. [CrossRef]
28. Seibert, J.; Stendahl, J.; Sørensen, R. Topographical influences on soil properties in boreal forests. *Geoderma* **2007**, *141*, 139–148. [CrossRef]
29. Bueno de Mesquita, C.P.; Tillmann, L.S.; Bernard, C.D.; Rosemond, K.C.; Molotch, N.P.; Suding, K.N. Topographic heterogeneity explains patterns of vegetation response to climate change (1972–2008) across a mountain landscape, Niwot Ridge, Colorado. *Arct. Antarct. Alp. Res.* **2018**, *50*, e1504492. [CrossRef]
30. Han, H.; Bai, J.; Ma, G.; Yan, J. Vegetation Phenological Changes in Multiple Landforms and Responses to Climate Change. *ISPRS J. Photogramm. Remote Sens.* **2020**, *9*, 111. [CrossRef]
31. Wang, G.; Peng, W. Quantifying spatiotemporal dynamics of vegetation and its differentiation mechanism based on geographical detector. *Environ. Sci. Pollut. Res.* **2022**, *29*, 32016–32031. [CrossRef]
32. Jung, S.; Park, J. Consistent Partial Least Squares Path Modeling via Regularization. *Front. Psychol.* **2018**, *9*, 174. [CrossRef] [PubMed]
33. Henseler, J.; Hubona, G.S.; Ray, P.A. Using PLS path modeling in new technology research: Updated guidelines. *Ind. Manag. Data Syst.* **2016**, *116*, 2–20. [CrossRef]
34. Schamberger, T.; Schuberth, F.; Henseler, J.; Dijkstra, T. Robust partial least squares path modeling. *Behaviormetrika* **2019**, *47*, 307–334. [CrossRef]
35. Rigdon, E.E. Rethinking Partial Least Squares Path Modeling: In Praise of Simple Methods. *Long Range Plan.* **2012**, *45*, 341–358. [CrossRef]
36. Rodrigues, V.S.; do Valle Junior, R.F.; Fernandes, L.S.S.; Pacheco, F. The assessment of water erosion using Partial Least Squares-Path Modeling: A study in a legally protected area with environmental land use conflicts. *Sci. Total Environ.* **2019**, *691*, 1225–1241. [CrossRef]
37. Chen, J. *Evolution and Water Resources Utilization of the Yangtze River*; Springer: Singapore, 2020; pp. 123–134.
38. Xu, X.; Hu, H.; Tan, Y.; Yang, G.; Zhu, P.; Jiang, B. Quantifying the impacts of climate variability and human interventions on crop production and food security in the Yangtze River Basin, China, 1990–2015. *Sci. Total. Environ.* **2019**, *665*, 379–389. [CrossRef]
39. Yue, Y. The Changes of Future Runoff and Drought and Floodin the Yangtze River Basin under Climate Change. Ph.D. Thesis, East China Normal University, Shanghai, China, 2022.
40. Li, Q. Study on Reconstructing Long-Term Terrestrial Water Storage Anomalies in the Yangtze River Basin and Analysis of Its Driving Factors. Ph.D. Thesis, China University of Geosciences, Wuhan, China, 2023.
41. Han, G.; Chen, J.; He, C.; Li, S.; Wu, H.; Liao, A.; Peng, S. A web-based system for supporting global land cover data production. *ISPRS J. Photogramm. Remote Sens.* **2015**, *103*, 66–80. [CrossRef]

42. Hengl, T.; Mendes de Jesus, J.; Heuvelink, G.B.; Ruiperez Gonzalez, M.; Kilibarda, M.; Blagotić, A.; Shangguan, W.; Wright, M.N.; Geng, X.; Bauer-Marschallinger, B.; et al. SoilGrids250m: Global gridded soil information based on machine learning. *PLoS ONE* **2017**, *12*, e0169748. [CrossRef]
43. Vannest, K.J.; Parker, R.I.; Davis, J.L.; Soares, D.A.; Smith, S.L. The Theil–Sen slope for high-stakes decisions from progress monitoring. *Behav. Disord.* **2012**, *37*, 271–280. [CrossRef]
44. Gocic, M.; Trajkovic, S. Analysis of changes in meteorological variables using Mann-Kendall and Sen's slope estimator statistical tests in Serbia. *Glob. Planet. Chang.* **2013**, *100*, 172–182. [CrossRef]
45. Döring, T.F.; Reckling, M. Detecting global trends of cereal yield stability by adjusting the coefficient of variation. *Eur. J. Agron.* **2018**, *99*, 30–36. [CrossRef]
46. Tatli, H. Detecting persistence of meteorological drought via the Hurst exponent. *Meteorol. Appl.* **2015**, *22*, 763–769. [CrossRef]
47. Gilmore, M.; Yu, C.; Rhodes, T.; Peebles, W. Investigation of rescaled range analysis, the Hurst exponent, and long-time correlations in plasma turbulence. *Phys. Plasmas* **2002**, *9*, 1312–1317. [CrossRef]
48. Sharma, P.N.; Shmueli, G.; Sarstedt, M.; Danks, N.; Ray, S. Prediction-oriented model selection in partial least squares path modeling. *Decis. Sci.* **2021**, *52*, 567–607. [CrossRef]
49. Tenenhaus, M.; Vinzi, V.E.; Chatelin, Y.M.; Lauro, C. PLS path modeling. *Comput. Stat. Data Anal.* **2005**, *48*, 159–205. [CrossRef]
50. Luo, J. Three-Dimensional Spatial and Temporal Characteristics of Soil pH and Acidification Driving Forces in Hubei, Hunan and Jiangxi Provinces. Master's Thesis, Huazhong Agricultural University, Wuhan, China, 2023.
51. Marcoulides, K.M.; Raykov, T. Evaluation of Variance Inflation Factors in Regression Models Using Latent Variable Modeling Methods. *Educ. Psychol. Meas.* **2019**, *79*, 874–882. [CrossRef]
52. Flinn, K.M.; Vellend, M.; Marks, P. Environmental causes and consequences of forest clearance and agricultural abandonment in central New York, USA. *J. Biogeogr.* **2005**, *32*, 439–452. [CrossRef]
53. Jin, X.; Wan, L.; Zhang, Y.; Schaepman, M. Impact of economic growth on vegetation health in China based on GIMMS NDVI. *Int. J. Remote Sens.* **2008**, *29*, 3715–3726. [CrossRef]
54. Wang, R.; Wang, Y.; Yan, F. Vegetation Growth Status and Topographic Effects in Frozen Soil Regions on the Qinghai-Tibet Plateau. *Remote Sens.* **2022**, *14*, 4830. [CrossRef]
55. Niu, Z.; Wang, L.; Fang, L.; Li, J.; Yao, R. Analysis of spatiotemporal variability in temperature extremes in the Yellow and Yangtze River basins during 1961–2014 based on high-density gauge observations. *Int. J. Climatol.* **2019**, *40*, 1–21. [CrossRef]
56. Fan, Z.; Luo, Q.; Yu, H.; Liu, J.; Xia, W. Spatial–Temporal Evolution of the Coupling Coordination Degree between Water and Land Resources Matching and Cultivated Land Use Eco-Efficiency: A Case Study of the Major Grain-Producing Areas in the Middle and Lower Reaches of the Yangtze River. *Land* **2023**, *12*, 982. [CrossRef]
57. Zhou, F.; Yao, M.; Fan, X.; Yin, G.; Meng, X.; Lin, Z. Evidence of warming from long-term records of climate and permafrost in the hinterland of the Qinghai–Tibet Plateau. *Front. Environ. Sci.* **2022**, *10*, 836085. [CrossRef]
58. Norsang, G.; Kocbach, L.; Tsoja, W.; Stamnes, J.; Dahlback, A.; Nema, P. Ground-based measurements and modeling of solar UV-B radiation in Lhasa, Tibet. *Atmos. Environ.* **2009**, *43*, 1498–1502. [CrossRef]
59. Zhang, A.; Li, X.; Zeng, F.; Jiang, Y.; Wang, R. Variation characteristics of different plant functional groups in alpine desert steppe of the Altun Mountains, northern Qinghai-Tibet Plateau. *Front. Plant Sci.* **2022**, *13*, 961692. [CrossRef]
60. Sun, Y.; Liu, S.; Shi, F.; An, Y.; Li, M.; Liu, Y. Spatio-temporal variations and coupling of human activity intensity and ecosystem services based on the four-quadrant model on the Qinghai-Tibet Plateau. *Sci. Total Environ.* **2020**, *743*, 140721.
61. Dai, X.; Wang, P.C. A new classification of large-scale climate regimes around the Tibetan Plateau based on seasonal circulation patterns. *Adv. Clim. Chang. Res.* **2017**, *8*, 26–36. [CrossRef]
62. Liu, X.; Yin, Z. Sensitivity of East Asian monsoon climate to the uplift of the Tibetan Plateau. *Palaeogeogr. Palaeoclimatol. Palaeoecol.* **2002**, *183*, 223–245. [CrossRef]
63. Yao, Y.; Zhang, B. A Preliminary Study of the Heating Effect of the Tibetan Plateau. *PLoS ONE* **2013**, *8*, e68750. [CrossRef]
64. Diao, C.; Liu, Y.; Zhao, L.; Zhuo, G.; Zhang, Y. Regional-scale vegetation-climate interactions on the Qinghai-Tibet Plateau. *Ecol. Inform.* **2021**, *65*, 101413. [CrossRef]
65. Shao, Z.; Ding, L.; Li, D.; Altan, O.; Huq, M.E.; Li, C. Exploring the relationship between urbanization and ecological environment using remote sensing images and statistical data: A case study in the Yangtze River Delta, China. *Sustainability* **2020**, *12*, 5620. [CrossRef]
66. Zhao, Y.; Yue, X.; Zhou, H.; Yu, Z.; Yuan, W. The effect of afforestation on a regional carbon sink: A case study in the Yangtze River Delta, China. *Environ. Res. Lett.* **2024**, *19*, 104064. [CrossRef]
67. Chen, D.; Jiang, P.; Li, M. Assessing potential ecosystem service dynamics driven by urbanization in the Yangtze River Economic Belt, China. *J. Environ. Manag.* **2021**, *292*, 112734. [CrossRef] [PubMed]
68. Zhang, D.; Wu, F.; Fang, Y.; Lu, N. Spatial and temporal variation Trend Analysis of vegetation cover in Urban agglomeration of Pearl River Delta from 2000 to 2015. In *Proceedings of the IOP Conference Series: Earth and Environmental Science*; IOP Publishing: Bristol, UK, 2020; Volume 615, p. 012028.

69. Wu, Y.; Wang, X.; Zhou, J.; Bing, H.; Sun, H.; Wang, J. The fate of phosphorus in sediments after the full operation of the Three Gorges Reservoir, China. *Environ. Pollut.* **2016**, *214*, 282–289. [CrossRef]
70. Wu, X.; Shen, Z.; Liu, R.; Ding, X. Land use/cover dynamics in response to changes in environmental and socio-political forces in the upper reaches of the Yangtze River, China. *Sensors* **2008**, *8*, 8104–8122. [CrossRef]
71. Xiao, L. Efficient population size of urban agglomerations in the Yangtze River Economic Belt from a financial perspective. *PLoS ONE* **2024**, *19*, e0311090. [CrossRef]
72. Peng, H.; Zhang, X.; Ren, W.; He, J. Spatial pattern and driving factors of cropland ecosystem services in a major grain-producing region: A production-living-ecology perspective. *Ecol. Indic.* **2023**, *155*, 111024. [CrossRef]
73. Yi, Y.; Hu, X.; Shi, C.; Kang, H.; Wang, B.; Zhang, C.; Liu, C. Vegetation dynamics and its relationship with climate factors in the middle reaches of the Yangtze River Based on MODIS NDVI. *Acta Ecol. Sin.* **2021**, *41*, 7796–7807.
74. Chen, S.; Guo, K.; Wu, F.; Wu, C. Analysis of the spatial and temporal characteristics of the winter precipitation in Southern China. *Clim. Chang. Res. Lett.* **2014**, *3*, 165–175. [CrossRef]
75. Liu, X.; Fan, Y.; Liu, P.; Wu, Q.; Hu, W.; Tian, K.; Huang, B. Characteristics of heavy metal pollution in farmland Soil of the Yangtze River economic belt based on bibliometric analysis. *Huan Jing Ke Xue = Huanjing Kexue* **2022**, *43*, 5169–5179.
76. Zheng, Z.; Qingyun, H. Spatio-temporal evaluation of the urban agglomeration expansion in the middle reaches of the Yangtze River and its impact on ecological lands. *Sci. Total Environ.* **2021**, *790*, 148150. [CrossRef]
77. Song, F.; Yang, X.; Wu, F. Suitable Pattern of the Natural Environment of Human Settlements in the Lower Reaches of the Yangtze River. *Atmosphere* **2019**, *10*, 200. [CrossRef]
78. Qin, B.; Zhu, G. The nutrient forms, cycling and exchange flux in the sediment and overlying water system in lakes from the middle and lower reaches of Yangtze River. *Sci. China Ser. D* **2006**, *49*, 1–13. [CrossRef]
79. Li, C.; Tian, Q.; Yu, R.; Zhou, B.; Xia, J.; Burke, C.; Dong, B.; Tett, S.F.; Freychet, N.; Lott, F.; et al. Attribution of extreme precipitation in the lower reaches of the Yangtze River during May 2016. *Environ. Res. Lett.* **2018**, *13*, 014015. [CrossRef]
80. Zhou, X.; Cai, J.; Xu, J.; Liu, S.; Wang, B.; Zhang, H.; Yue, L.; Wu, L.; Wu, Y.; Chen, D. Climate regulates the effect of land-use change on the diversity of soil microbial functional groups and soil multifunctionality. *J. Appl. Ecol.* **2024**, *61*, 2087–2099. [CrossRef]
81. Long, H. Analysis of the key factors of ecological environment protection in the national economic sustainable development goals. *J. Environ. Public Health* **2022**, *2022*, 3593587. [CrossRef]
82. Zhang, X.; Li, Y.; Wang, G.; Zhang, H.; Yu, R.; Li, N.; Zheng, J.; Yu, Y. Soil quality assessment in farmland of a rapidly industrializing area in the Yangtze Delta, China. *Int. J. Environ. Res. Public Health* **2022**, *19*, 12912. [CrossRef]
83. Wang, X.; Zhang, Z.; Hao, H.; Zhang, C.; Wang, D. Analysis on the effects of ecological conservation redline policies in the Pearl River Delta area, China. *Front. Ecol. Evol.* **2023**, *11*, 1164602. [CrossRef]
84. Yu, Y.; Zhao, W.; Martinez-Murillo, J.F.; Pereira, P. Loess Plateau: From degradation to restoration. *Sci. Total Environ.* **2020**, *738*, 140206. [CrossRef]
85. Chen, D.; Li, Q.; He, F.; Chen, X.; Xu, S.; Zhao, X.; Li, J.; Liu, L.; Zhao, L. Restoration Measures Supported Surface Soil Carbon and Nitrogen Density in Alpine Grassland of Sanjiangyuan Region, China. *Pol. J. Environ. Stud.* **2020**, *29*, 3071–3083. [CrossRef]
86. Wen, B.; Liu, C.; Tian, X.; Zhang, Q.; Huang, S.; Zhang, Y. Interactive Effects of Ecological Land Agglomeration and Habitat Quality on Soil Erosion in the Jinsha River Basin, China. *Land* **2024**, *13*, 229. [CrossRef]
87. Yang, H.; Zhong, X.; Deng, S.; Xu, H. Assessment of the impact of LUCC on NPP and its influencing factors in the Yangtze River basin, China. *Catena* **2021**, *206*, 105542. [CrossRef]
88. Xu, L.; Yu, G.; Tu, Z.; Zhang, Y.; Tsendbazar, N.E. Monitoring vegetation change and their potential drivers in Yangtze River Basin of China from 1982 to 2015. *Environ. Monit. Assess.* **2020**, *192*, 642. [CrossRef] [PubMed]
89. Jombart, T.; Dray, S.; Dufour, A.B. Finding essential scales of spatial variation in ecological data: A multivariate approach. *Ecography* **2009**, *32*, 161–168. [CrossRef]
90. Xie, D.; Zhang, J.; Sun, P.; Pan, Y.; Yun, Y.; Yuan, Z. Remote sensing data fusion by combining STARFM and downscaling mixed pixel algorithm. *J. Remote Sens.* **2016**, *20*, 62–72.

Disclaimer/Publisher's Note: The statements, opinions and data contained in all publications are solely those of the individual author(s) and contributor(s) and not of MDPI and/or the editor(s). MDPI and/or the editor(s) disclaim responsibility for any injury to people or property resulting from any ideas, methods, instructions or products referred to in the content.